Heliyon 9 (2023) e14341

Contents lists available at ScienceDirect

Heliyon

journal homepage: www.cell.com/heliyon

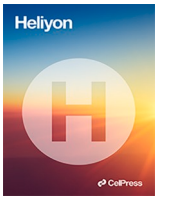

Research article

Facile synthesis and characterization of multi-walled carbon nanotubes decorated with hydroxyapatite from cattle horns for adsorptive removal of fluoride

Walter Ojok [a,b,f,*], James P Bolender [c], John Wasswa [d], Emmanuel Ntambi [a], William Wanasolo [e], Brenda Moodley [f]

[a] Department of Chemistry, Faculty of Science, Mbarara University of Science and Technology, P.O Box 1410, Mbarara, Uganda
[b] Department of Chemistry, Faculty of Science, Muni University, P.O Box 725, Arua, Uganda
[c] Department of Chemistry and Biochemistry, University of San Diego, 5998 Alcala Park, San Diego, CA 92110, USA
[d] Department of Chemistry, College of Natural Sciences, Makerere University, P.O Box 7062, Kampala, Uganda
[e] Department of Chemistry, Faculty of Science, Kyambogo University, P.O Box 1 Kyambogo, Kampala, Uganda
[f] School of Chemistry and Physics, University of KwaZulu-Natal, Westville Campus, Durban, 4000, South Africa

ARTICLE INFO

Keywords:
Cattle horn
Fluoride adsorption
Hydroxyapatite
Kinetics
Multi-walled carbon nanotubes
Response surface methodology

ABSTRACT

Developing a new adsorbent for fluoride removal from cattle horn waste materials by a facile chemical method has shown great potential for fluoride removal. This paper reports the synthesis of multi-walled carbon nanotubes decorated with hydroxyapatite from cattle horns (MWCNT-CH) using a facile chemical method. Characterization studies using standard techniques showed that the composite is mesoporous with a rough morphology and contained MWCNTs uniformly encapsulated by the hydroxyapatite forming a crystalline MWCNT-CH composite. Optimization of fluoride adsorption by the as-synthesized composite using Response Surface Methodology (RSM) showed that a maximum fluoride removal efficiency of 80.21% can be attained at initial fluoride concentration = 10 mg/L, pH = 5.25, adsorbent dose = 0.5 g and a contact time of 78 min. ANOVA indicates contribution of the process variables in descending order as pH > contact time > adsorbent dose > initial fluoride concentration. Langmuir isotherm (R^2 = 0.9991) best described the process, and the maximum adsorption capacity of fluoride onto the as-synthesized MWCNT-CH composite was 41.7 mg/g. Adsorption kinetics data were best fitted in the pseudo-second-order kinetic model (R^2 = 0.9969), indicating chemisorption. The thermodynamic parameter (Δ H = 13.95 J/mol and Δ S = 65.76 J/mol/K) showed that fluoride adsorption onto the MWCNT-CH composite was a spontaneous, endothermic, and entropy-driving process. Moreover, the adsorption mechanism involves ion exchange, electrostatic interaction, and hydrogen bonding. Fluoride was successfully desorbed (using 0.1 M NaOH) from the composite in four cycles, retaining fluoride removal efficiency in the fourth cycle of 57.3%.

* Corresponding author. Department of Chemistry, Faculty of Science, Mbarara University of Science and Technology, P.O Box 1410, Mbarara, Uganda.
E-mail address: w.ojok@muni.ac.ug (W. Ojok).

https://doi.org/10.1016/j.heliyon.2023.e14341
Received 19 December 2022; Received in revised form 1 March 2023; Accepted 1 March 2023
Available online 9 March 2023

1. Introduction

Green chemistry routes to synthesizing carbon-based nanomaterials, including functionalized carbon nanotubes, have drawn considerable attention due to their superior physicochemical characteristics [1,2]. This is attributed mainly to their unique physical, chemical, and mechanical properties, with interior voids and exterior surfaces exposed for use in several applications.

Carbon nanotubes loaded with other nanoparticles are now regarded as a new class of multifunctional materials with diverse applications [3,4]. Standard methods for decorating CNTs include chemical vapor deposition, thermal treatments, and interaction of CNTs with already prepared suspensions of other nanoparticles [5].

On the other hand, the adsorption properties and removal efficiency of toxic ions, such as fluoride ions from water using nanoparticles, have attracted enormous research over the years. Fluoride is a significant contaminant of groundwater resources affecting over 200 million people globally [6,7]. In the range of 0–1.0 mgL^{-1}, fluoride is an essential mineral ion for the mineralization of bones and teeth. However, at concentrations above 1.5 mgL^{-1}, fluoride is known to cause morbidity, including dental and skeletal fluorosis. Therefore, many methods have been applied to remove fluoride ions from water. These include ion exchange, chemical coagulation, precipitation, electrochemical methods, and adsorption technique [8]. Amongst these methods, the adsorption technique is auspiciously selected for removing fluoride ions from the aqueous solution because of its advantages, such as low cost, low energy consumption, and ease of operation. However, the practical applicability of adsorption depends on the adsorbent's efficiency, cost performance, and regeneration ability. Various adsorbents, including carbon, biomass, activated alumina, hydroxyapatite, and metal oxide composites, have been studied but showed slow adsorption kinetics and low efficiency/high production cost [9]. Hence, searching for an effective, environmentally compatible, and economically viable adsorbent for sustainable fluoride removal remains paramount.

Although MWCNTs have good adsorption property towards fluoride, their superhydrophobic nature presents a challenge due to aggregation in aqueous media [5,9]. This affects the adsorption efficiency of MWCNTs due to the intermolecular interactions between adjacent CNTs, which brings about aggregation and reduced accessible surface area [9]. This calls for their functionalization. Consequently, several studies have been reported on the functionalization of CNTs with metal oxide nanoparticles [10], metal nanoparticles [11], chitosan [12], ionic liquids [13], hydroxyapatite [14], polymers [15] and graphene [3]. Hydroxyapatite (HAp) is a cheap mineral in animal skeletal materials, including cattle horns with good fluoride removal ability due to its rich calcium content. A simple and effective method of functionalizing MWCNTs with HAp by in situ deposition of HAp to improve their hydrophilicity and biocompatibility was reported by several researchers [9,14,16]. Cattle horn waste is an abundant material that is rich in hydroxyapatite [17,18]. Daily, a large amount of cattle horn waste is produced in abattoirs and beef processing factories. This waste contains organic matter that supports microbial growth and can become environmental hazards in landfills. Its rich mineral composition could enhance fluoride sorption capacity of the composite [18]. Therefore, the current study attempts to develop a biocomposite from cattle horn waste and graphite by a facile chemical method and optimize its fluoride adsorption ability using central composite design (CCD).

Research on the functionalization of MWCNTs with HAp for its application for the adsorption of fluoride from water is still nascent. Furthermore, no literature on the synthesis of MWCNTs decorated with HAp from cattle horns is available. Therefore, this study reports for the first-time synthesis of MWCNTs functionalized with an aqueous extract of cattle horns containing HAp and conduct batch experimental investigations for process variable optimization by implementing the CCD approach in RSM.

In this study, we report a novel chemical method for synthesizing MWCNTs/HAp composite using cattle horn extract. This method of MWCNT synthesis does not require the use of metal catalysts and high temperatures, making it a cheap and environmentally friendly route to MWCNTs without the need to remove metal impurities. Furthermore, HAp from cattle horns used in functionalization is cheap because cattle horns are widely available. Functionalization of MWCNTs with hydroxyapatite from cattle horn by co-precipitation makes the synthesis process green since both materials are abundant biomass in the environment. Hence the main objectives of the current study were to:

i) Synthesize MWCNTs decorated with hydroxyapatite from cattle horn extract (MWCNT-CH) and characterize them by BET surface analyzer, Zeta potential analyzer, XRD, FTIR, SEM, and TEM
ii) Study efficiency of as-synthesized MWCNTs-CH composite in fluoride adsorption from water by batch method.
iii) Optimize fluoride adsorption using the as-synthesized MWCNT-CH composite using response surface methodology and develop a model for predicting the fluoride adsorption process.

2. Materials and methods

2.1. Materials

All chemicals were of analytical grade. Sodium fluoride (NaF), nitric acid (65%), sulphuric acid (98%), and hydrochloric acid (HCl, 36%) were purchased from Merck, Darmstadt, Germany. Sodium chloride (NaCl), sodium nitrate ($NaNO_3$), sodium sulphate (Na_2SO_4), sodium phosphate (Na_3PO_4), potassium hydrogen carbonate ($KHCO_3$), graphite powder, and Total ionic strength adjustment buffer (TISAB) were obtained from Sigma Aldrich Co. USA. Deionized water was used for the preparation of solutions. Cattle horn was obtained from an abattoir in Mbarara city, Uganda.

2.2. Synthesis of MWCNT-CH composites

2.2.1. Preparation of CNTs

CNTs were prepared from graphite by the chemical method [2] (Fig. 1). First, graphite powder (5.0 g) in water (5.0 mL) was added slowly to a mixture of nitric acid (25 mL)/sulphuric acid (50 mL), and the mixture was homogenized by stirring for 30 min. Next, the mixture was cooled to 0 °*C* in an ice bath, then sodium nitrate (25.0 g) was slowly and carefully added to the mixture at 0 °*C* with magnetic stirring for 30 min. The solution was then heated up to 70 °*C* for 24 h and then placed in the air for three days at ambient temperature without filtering. The first and second floating layers were collected and washed thoroughly with distilled water under magnetic stirring for 1 h and then filtered. The collected CNTs were then dried for 3 h at 50 °*C* in an air oven.

2.2.2. Synthesis of MWCNTs

MWCNTs were prepared from the as-synthesized CNTs using previously reported methods [13] (Fig. 1). Briefly, CNTs (0.317 g) were added to a mixture of concentrated nitric acid (65%) and concentrated sulphuric acid (98%) in a ratio of 1:3 by volume and ultrasonicated for 5 min. The mixture was then refluxed for 5 h at 60 °*C*. Subsequently, the solid products were filtered and then washed with distilled water to remove the acid residue and dried in an air vacuum at 70 °*C* to get MWCNTs.

2.2.3. Decoration of MWCNTs with hydroxyapatite

Hydroxyapatite was obtained by digesting dried cattle horns with 25% sodium hydroxide [19]. The obtained solution containing hydroxyapatite was added slowly onto the as-synthesized MWCNTs with constant stirring and allowed to stand for 1 h at 45 °*C*. The pH of the mixture was adjusted to 10 by adding an ammonium hydroxide solution. The mixture obtained was aged for 24 h at room temperature to form colloids. The colloids were centrifuged, washed with distilled water several times until pH 7, dried at 80 °*C* in an air oven, and finally calcined at 200 °*C* for 2 h to form MWCNTs decorated with hydroxyapatite (MWCNT-CH) and then eventually sealed in glass containers for subsequent use. The scheme summarizing the process is given in Fig. 1.

2.3. Characterization methods

An x-ray powder diffractometer (XRD, D8 ADVANCE X, Germany) with Cu-Kα (40 kV, 40 mA) radiation at a scanning rate of 8 °/minute in the 2 θ diffraction angle in the scanning range of 10–80 ° was used to study the phase composition and crystal structure of the as-synthesized MWCNTs and MWCNTs/HAp. The chemical structure was studied using a Fourier transform infrared spectrometer ((PerkinElmer, UK equipment) in the wave number range of 400–4000 cm^{-1}. Surface morphology was characterized by a Scanning electron microscope (FESEM, ZEISS, Germany) at an accelerating voltage of 5 kV. Elemental composition was determined by Energy dispersive spectroscopy (EDS). Transmission electron microscopy (TEM) was achieved at an accelerating voltage of 200 keV on a G2

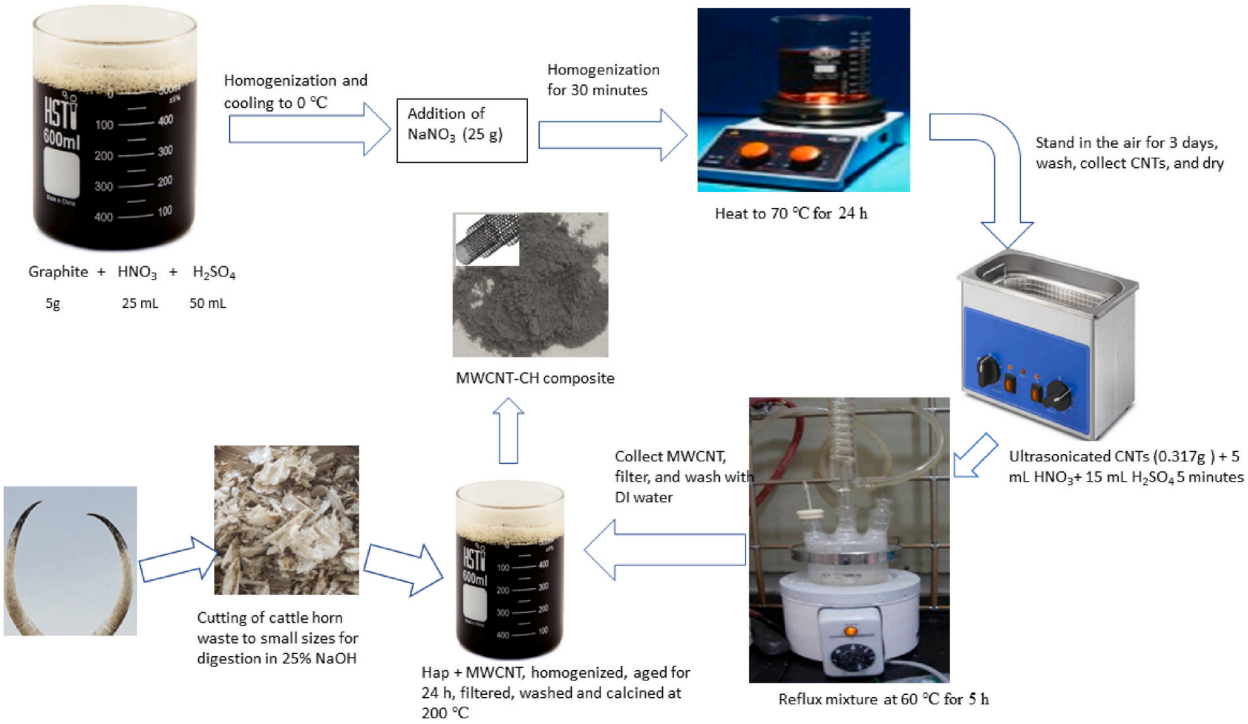

Fig. 1. Schematic illustration of the facile synthesis of MWCNT-CH composite.

F20, TWIN Cryo-TEM (Phillips, Netherlands) instrument. A Micro metrics Tristar II surface area and porosity analyzer determined the specific surface areas, pore size distribution, and total pore volume was calculated using the Brunauer-Emmett-Teller (BET) and the Barrett-Joyner-Halenda (BJH) equation from the N_2 adsorption-desorption isotherms. The Fourier-transformed infrared spectrometer (PerkinElmer, UK equipment) was used to study the chemical structure of the composites in the wavenumber range 400–4000 cm^{-1}.

2.4. Fluoride adsorption experiments

Batch adsorption experiments were conducted with a 25 mL fluoride solution of known concentration in 50 mL bottles. The bottles were placed in an orbital incubator at 25 $^{\circ}C$ and at a speed of 300 rpm for 2h. Adsorbent dosage was studied from 0.05 to 0.50 g, contact time from 1 to 360 min, pH (3.0–12), and initial fluoride concentration of 10–100 mg/L. One parameter was studied at a time while keeping the others constant for each of the adsorbents, and residual fluoride concentration in the filtrate was determined using a calibrated Platinum series fluoride electrode (Model 51928–88, HACH Co., Ltd, Loveland, Colorado, U.S.A.) using EPA method 9124 [20].

Adsorption kinetic experiments were performed at different contact times from 1 to 360 min with an adsorbent dosage of 1.0 g and an initial fluoride concentration of 10 mg/L at pH 6. In addition, equilibrium isotherm was studied by varying initial fluoride concentration from 2 to 100 mg/L at pH 6. Lastly, the adsorption efficiency and adsorption capacity of the as-synthesized MWCNT-CH composite in removing fluoride from aqueous media were calculated using Eqs 1and 2 [21]:

$$Fluoride\ removal\ (\%) = \frac{C_0 - C_e}{C_o} \text{ x } 100 \tag{1}$$

$$Adsorption\ capacity, Q = \frac{V\ x\ (C_o - C_e)}{1000\ x\ m} \tag{2}$$

Where V (mL) is volume of solution, m (g) is the mass of MWCNT used while $C_0$and C_e were the initial fluoride concentration and equilibrium fluoride concentration in mg/L.

The MWCNT-CH composite (2 g) was shaken at 180 rpm with a fluoride solution (10 mg/L) to study its adsorption and reusability for fluoride removal. In this experiment, 100 mL of the fluoride solution was shaken at 180 rpm for 12 h to attain equilibrium, and residual fluoride was determined, as described earlier. After the adsorption experiment in the first cycle, the spent adsorbent was separated by centrifuging, and the residue was agitated with 0.1 M NaOH solution for 1h. Lastly, the residue was dried at 110 °C and used in additional adsorption experiments using the same procedure described in this section. The adsorbent was regenerated four times in this experiment, with three replications in each case.

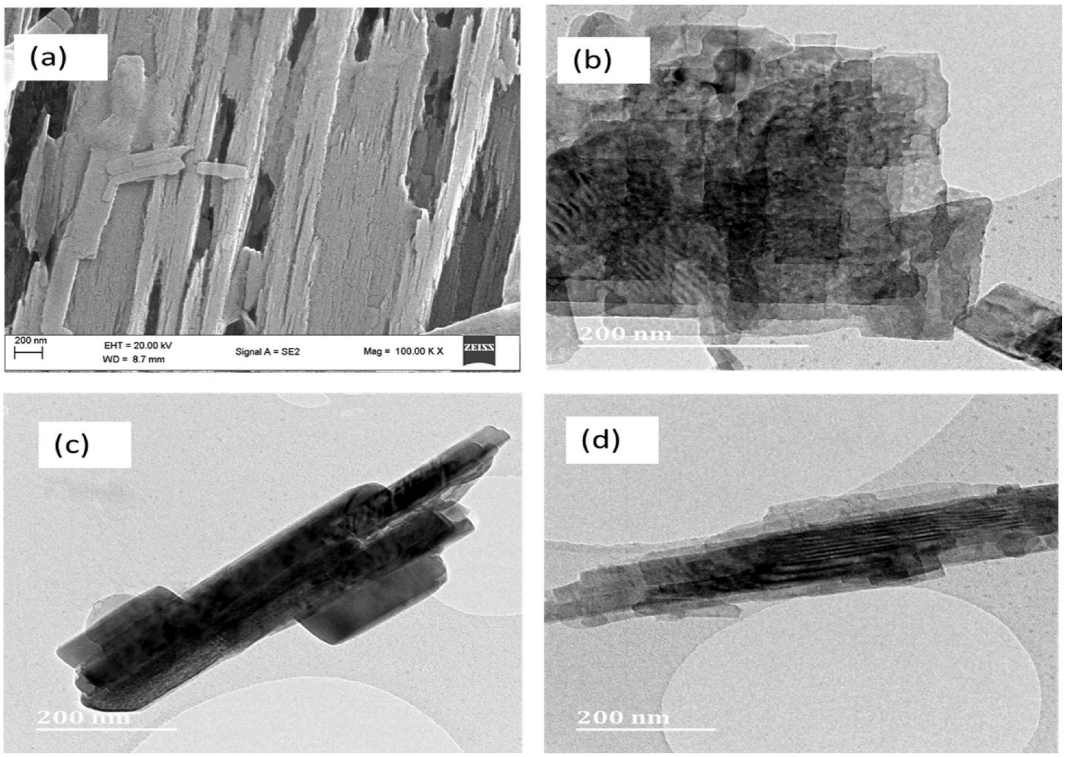

Fig. 2. (a) SEM micrograph (b, c, d) TEM images of some of the MWCNT-CH composite.

The effect of co-existing anions SO_4^{2-}, NO_3^-, Cl^-, PO_4^{3-}, and HCO_3^- on fluoride removal using the as-synthesized MWCNT-CH composite was studied by adding the co-existing anions (25 mL, 0.01 M) to fluoride solution (25 mL, 10 mg/L). The resulting solution was shaken with 0.5 g of the as-synthesized MWCNT-CH composite for 12 h, and residual fluoride was determined, as described earlier in this section.

2.5. Response surface methodology experimental design

Response Surface Methodology was used to design the experimental matrix to minimize wastage using fewer experiments [22,]. In this study, the experimental design and the interactive effects of the process variables on the removal efficiency of fluoride ions by the as-synthesized MWCNT-CH composite were modeled using the Central Composite Design (CCD) in Design Expert Software (Version 13.0.0, Stat-Ease Inc. Minneapolis, Minnesota, USA). The variables considered were initial fluoride concentration (A), contact time (B), pH (C), and adsorbent dose (D) on fluoride removal efficiency by the as-synthesized MWCNT-CH composite and percentage fluoride removal as the response. A total of thirty experimental runs were designed based on the 2^n factorial points, 2n axial points, and n center points (6 replications), that is

$$\text{Number of experiments}, N = 2^n + 2n + 6 \quad (3)$$

3. Results and discussion

3.1. Surface morphology of the MWCNT-CH composite

From the SEM microscopic examination (Fig. 2. (a), the MWCNT-CH composite had twisted and clustered CNTs with a rough morphology. However, some adjacent parts of the MWCNT-CH composite were stacked together, as seen in the TEM images in Fig. 2 (b, c, d), creating a flake-like orientation. Again, as seen from TEM images (Fig. 2 (c), the MWCNTs were uniformly encapsulated by the hydroxyapatite (Hap) from cattle horns (CH) to form an MWCNT-CH composite. The energy dispersive X-ray spectroscopy results in Fig. 3 (a) and (b) show that the prominent elemental peaks in the MWCNT-CH were due to S, Ca, O, C, and P. The high proportion of Ca, S, O, and P in the composite is from the cattle horn core, while carbon is from the MWCNT. The F peak in the EDX spectrum in Fig. 3 (b) and F in the EDX elemental mapping in Fig. 4 (b) while it was absent in Fig. 4(a) shows the ability of the MWCNT-CH composite to remove fluoride ions from water.

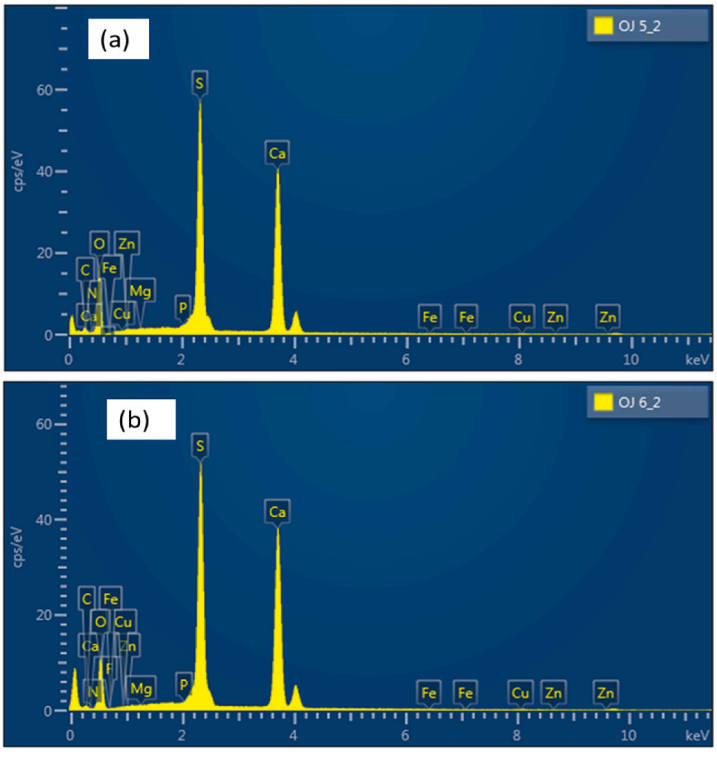

OJ 5_2	Wt%	Wt% Sigma
C	7.66	0.74
N	0.00	1.25
O	45.66	0.50
F	0.00	0.06
Mg	0.09	0.05
P	0.31	0.06
S	21.32	0.24
Ca	24.61	0.27
Fe	0.00	0.06
Cu	0.35	0.09
Zn	0.00	0.10
Total	100.00	

OJ 6_2	Wt%	Wt% Sigma
C	6.12	1.45
N	0.00	2.01
O	42.04	0.77
F	0.61	0.51
Mg	0.02	0.05
P	0.40	0.07
S	23.60	0.42
Ca	27.00	0.48
Fe	0.02	0.07
Cu	0.30	0.10
Zn	0.00	0.11
Total	100.00	

Fig. 3. EDX spectra of the MWCNT-CH biocomposite (a) before fluoride sorption (b) after fluoride sorption.

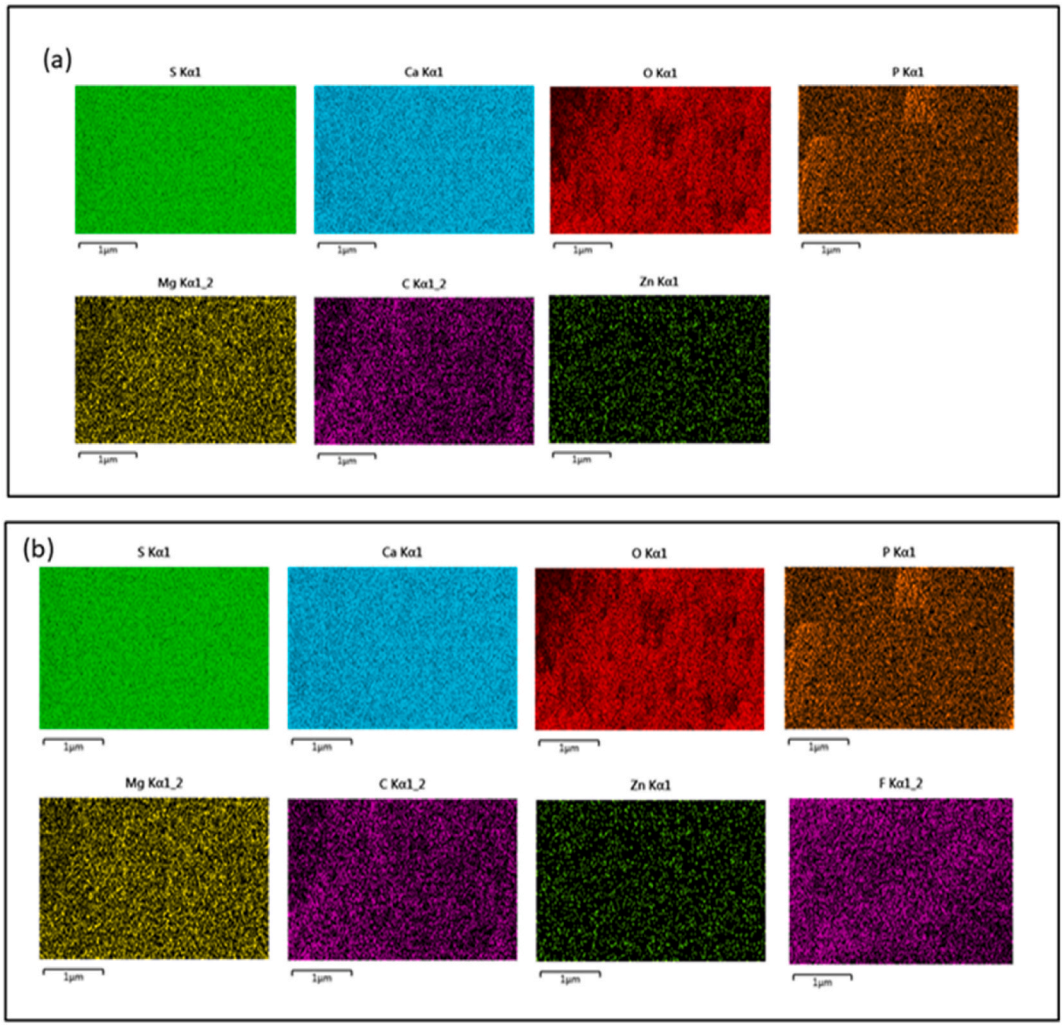

Fig. 4. Energy dispersive X-ray spectroscopy (EDX) Elemental mapping for (a) MWCNT-CH before fluoride removal and (b) MWCNT-CH after fluoride removal.

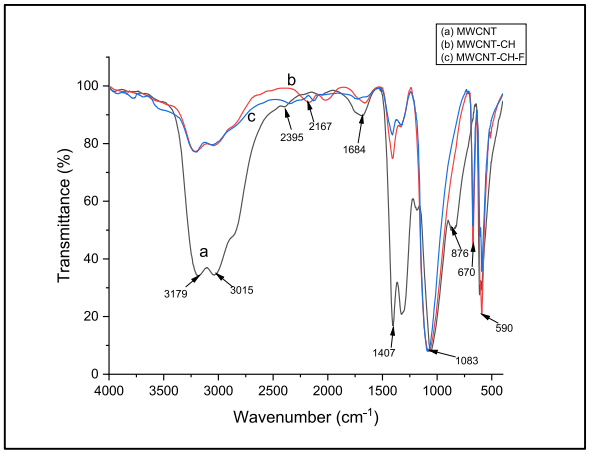

Fig. 5. FTIR spectra of (a)MWCNTs (b) MWCNT-CH (c) MWCNT–CH–F.

3.2. FTIR spectroscopic analysis of the MWCNT-CH composite

FTIR spectroscopic analysis of MWCNTs, MWCNTs-CH, and MWCNTs/CH–F are depicted in Fig. 5. The broad peaks at 3000–3320 cm^{-1} are assigned to the hydroxyl stretching vibration in the COOH group associated with the MWCNT composites. While the weak peak observed at 2800 cm^{-1} is assigned to the asymmetric/symmetric stretching vibration of methylene groups, and that at 1684 cm^{-1} was due to the asymmetric stretching vibration of the C═O in the carbon nanotube structure. The peak at 1083 cm^{-1} was due to C–O–C groups, while C–H bonds in MWCNTs, MWCNT/CH, and MWCNT/CH–F (Fig. 5).

For MWCNT/CH and MWCNT/CH–F, additional peaks occurred at 876 cm^{-1} assigned to CO_3^{2-} while those at 590 and 670 cm^{-1} were due to PO_4^{3-} group in the composite. The disappearance of the peak at 876 cm^{-1} and reduction of the C═O peak at 1684 cm^{-1} in the MWCNT/CH and further in MWCNT/CH–F indicates the participation of the –COOH group in binding to the hydroxyapatite to form the composite and role of the composite in fluoride removal.

3.3. X-ray diffraction study of the MWCNT-CH composite

The XRD pattern of the as-synthesized MWCNT-CH composite given in Fig. S1(supporting information) shows the presence of a prominent diffraction peak at 25.53 °. This peak indicates the diffraction plane (002) for MWCNT in the composite [2]. This plane corresponds to the spacing of the carbon nanotube interlayers. The peak around 10 ° was due to the graphene oxide formed during synthesizing the composite (ICDD 01–071 - 4630). The characteristic diffraction peaks for crystalline hydroxyapatite phases can be seen at 26.3 °, 33.6 °, 35 °, 38.9 °, and 41 ° which appeared in the MWCNT-CH (Fig. S1, supporting information), which are in agreement with the standard ICCD card for hydroxyapatite (ICCD 01-074-0566). This indicates the successful decoration of MWCNT with hydroxyapatite from cattle horns. The prominent peak at 25.52 ° was used to calculate the crystallite size, L, of the MWCNT-CH composite, using the Debye-Scherrer formula (Eqn. (4))

$$L = \frac{k\lambda}{\beta \cos \Theta} \tag{4}$$

The crystallite size, L, calculated for the peak at 25.53 °, was 3.84 nm which is higher than that obtained in a study by David et al. (2021). Furthermore, intermediate peaks at 33.6 °, 38.9 °, and 41 ° further confirm the presence of MWCNT-CH. The XRD spectrum obtained indicates that in addition to the MWCNT peak at 25.53 °, other peaks were introduced due to the functionalities in the cattle horn extract.

3.4. Brunauer-Emmett-Teller (BET) and Barret-Joyner-Hallender (BJH) analysis of the MWCNT-CH composite

A nitrogen adsorption study was conducted to study the surface area and textural nature of the MWCNT-CH composite and depicted a typical type III isotherm in Fig. S2 (supporting information). The BJH pore size distribution curves obtained from the adsorption branches indicate a pore size of 0.99 nm. The BET-specific surface area and total pore volume of the MWCNT-CH composite were 0.2643 cm^2/g and 0.00062 cm^3/g, respectively. The surface area for the composite is lower than that obtained for the CNT-Hap composite in a study by Tang et al. (2018). This may be attributed to the failure of the alkaline hydrolysis of the cattle horn waste to leach enough hydroxyapatite for functionalizing the CNTs.

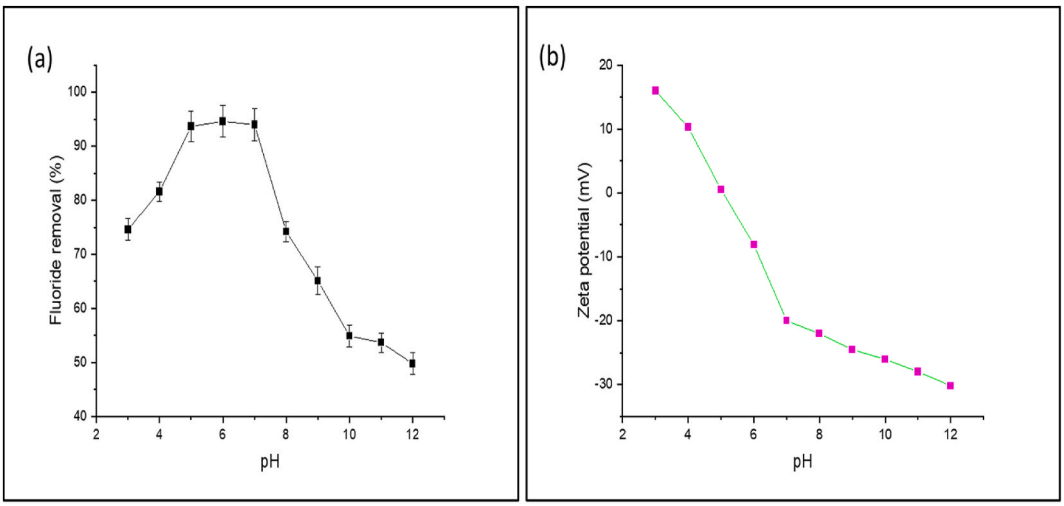

Fig. 6. (a) Effect of pH on fluoride removal using MWCNT-CH composite (b)variation of Zeta potential of MWCNT-CH with pH.

3.5. Fluoride ion removal from aqueous solution

3.5.1. Fluoride ion adsorption onto MWCNT-CH composite at different pH and zeta potential measurements

Fluoride adsorption onto the as-synthesized MWCNT-CH was studied at pH values from 3 to 12 (Fig. 6). Fluoride adsorption increased rapidly in the pH range of 3–5, then maintained maximum capacity from pH 5–7 but decreased when pH increased beyond 7 (Fig. 6 (a), while the zeta potential generally decreased with an increase in pH (Fig. 6 (b). In acidic conditions, the surface of the MWCNT-CH composite was protonated for electrostatic interaction with fluoride ions [23]. Therefore, a pH value of 7 was selected as the optimum for subsequent adsorption experiments.

On the contrary, the percentage of fluoride removed decreased in the alkaline pH range due to the saturation of the active sites with negative charges, which restrained the diffusion of fluoride ions on the adsorbent surface. Our results are consistent with related works, which reported high fluoride adsorption capacities in acidic media attributable to anionic $\pi-$ electrostatic interaction with the protonated adsorbent surfaces and a low fluoride removal efficiency in alkaline media as a result of repulsion of fluoride ions by the negatively charged adsorbent surface (Alhassan et al., 2020; He et al., 2020). This is consistent with the decrease in zeta potential with an increase in pH observed, revealing that the electrical charge on the surface of the MWCNT-CH composite depended on the pH of the media [24]. This is because the surface of the composite was protonated in acidic media and deprotonated in alkaline media.

3.5.2. Kinetic studies of fluoride adsorption onto MWCNT-CH composite

The amount of fluoride removed increased rapidly in the first 50 min, then gradually increasing contact time until equilibrium was reached at about 80 min for the various initial fluoride concentrations (10, 50, and 100 mg/L). The initial rapid increase in fluoride adsorption is due to the availability of active sites. The slow fluoride adsorption after 50 min was a result of the saturation of the active sites on the MWCNT-CH composite (Fig. 7(a). Based on this result, 80 min was selected as the optimum equilibration time for further experiments.

The adsorption data were fitted into the Lagergren Pseudo-first order, pseudo-second order, Elovich, and Weber Morris kinetic models.

Equations (4)–(7) give the linearized forms of the Lagergren pseudo-first order, pseudo-second order, Moris-Weber Intra-particle diffusion, and Elovich kinetic models, and corresponding plots for the models are shown in Fig. 7 with corresponding kinetic parameters and linear regression correlation coefficients (R^2) given in Table 1.

The pseudo-first-order model can be presented as shown in equation (5) [25]

$$\ln(Q_e - Q_t) = lnQ_e - k_1 t \tag{5}$$

Where Q_e and Q_t are equilibrium adsorption capacity and amount of fluoride sorbed at time t (minutes), respectively, and k_1 is the rate

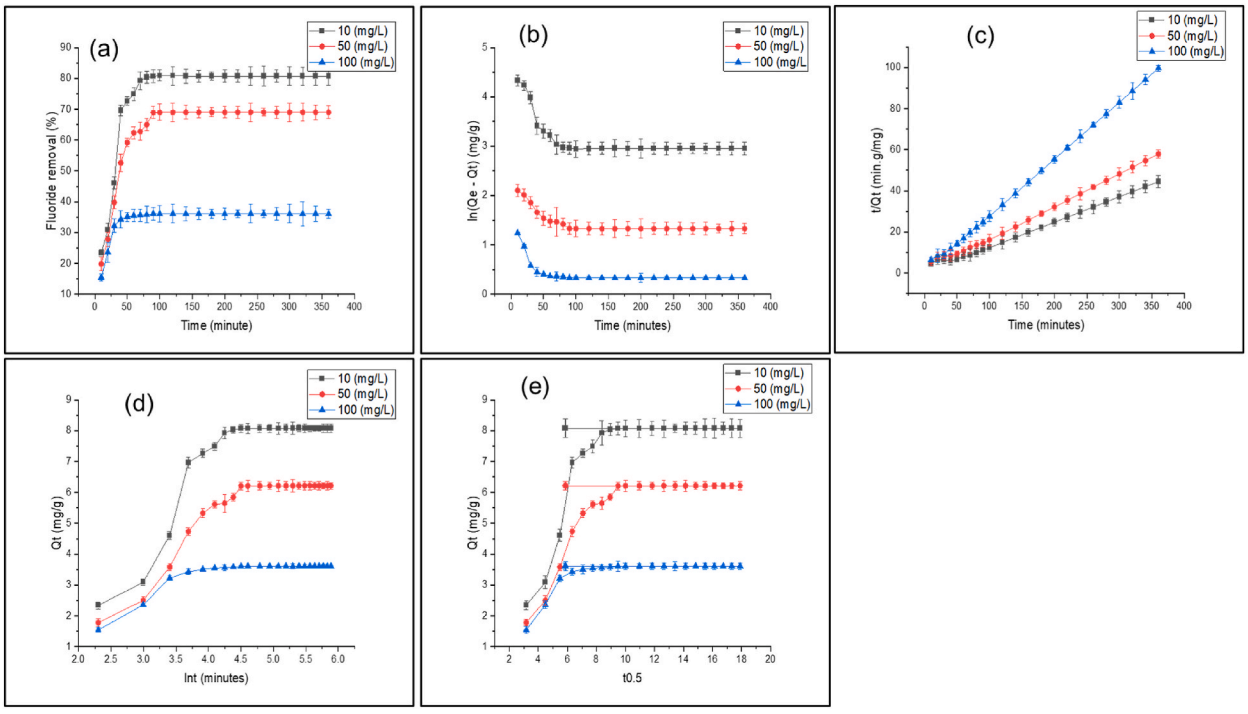

Fig. 7. (a) Effect of contact time on the adsorption process at different initial fluoride concentrations (b) Lagergren pseudo-first-order kinetic (c) Lagergren pseudo-second-order kinetic (d) Elovich kinetic (e) Weber-Morris intra-particle diffusion.

Table 1
Kinetics parameters for the adsorption of fluoride onto the as-synthesized MWCNT- CH composite.

Kinetic model	Initial fluoride concentration (mg/L)	Kinetic constant	$Q_{e.exp}$ ($mg.g^{-1}$)	$Q_{e.cal}$ ($mg.g^{-1}$)	R^2
Pseudo-first order	10	00 -0.00236 min^{-1}	8.08	34.56	0.35208
	50	−0.00137 min^{-1}	6.2	5.348	0.41106
	100	−0.00105 min^{-1}	3.673	1.8	0.23347
Pseudo-second order	10	0.01043 g mg^{-1}.min	8.08	8.48	0.9952
	50	0.01056 g mg^{-1}.min	6.2	6.567	0.9962
	100	0.06440 g mg^{-1}.min	3.61	3.673	0.9993
Intra-particle diffusion	10	K_{id} = 0.27228			0.35332
	50	K_{id} = 0.18447			0.41089
	100	K_{id} = 0.05946			0.26459
	Initial Fluoride conc. (mg/L)	**β**	**α**		**R^2**
Elovich	10	0.715	2.087		0.73557
	50	0.8886	6.957		0.75537
	100	2.6182	83.625		0.73572

constant. A plot of $\ln(Q_e - Q_t)$ against t is used to determine the kinetic parameters.

A linearized form of the pseudo-second-order model is defined by equation (6) [26]

$$\frac{t}{Q_t} = \frac{1}{Q_e^2 k_2} + \frac{t}{Q_e} \tag{6}$$

where Q_e and Q_t are equilibrium adsorption capacity and amount of fluoride sorbed at time t (minutes), respectively, and k_2 is the rate constant. A plot of $\frac{t}{Q_t}$ against t is used to determine the model parameters.

Diffusion process affects the transfer of adsorbate onto the adsorbent sites and is studied using the Weber-Morris equation (5) [27–29].

The model relates the amount of solute sorbed onto the adsorbent, Q_t, as being proportional to the square root of contact time, t, for the adsorption process as given in equation (7) [29]:

$$Q_t = k_{id} t^{0.5} \tag{7}$$

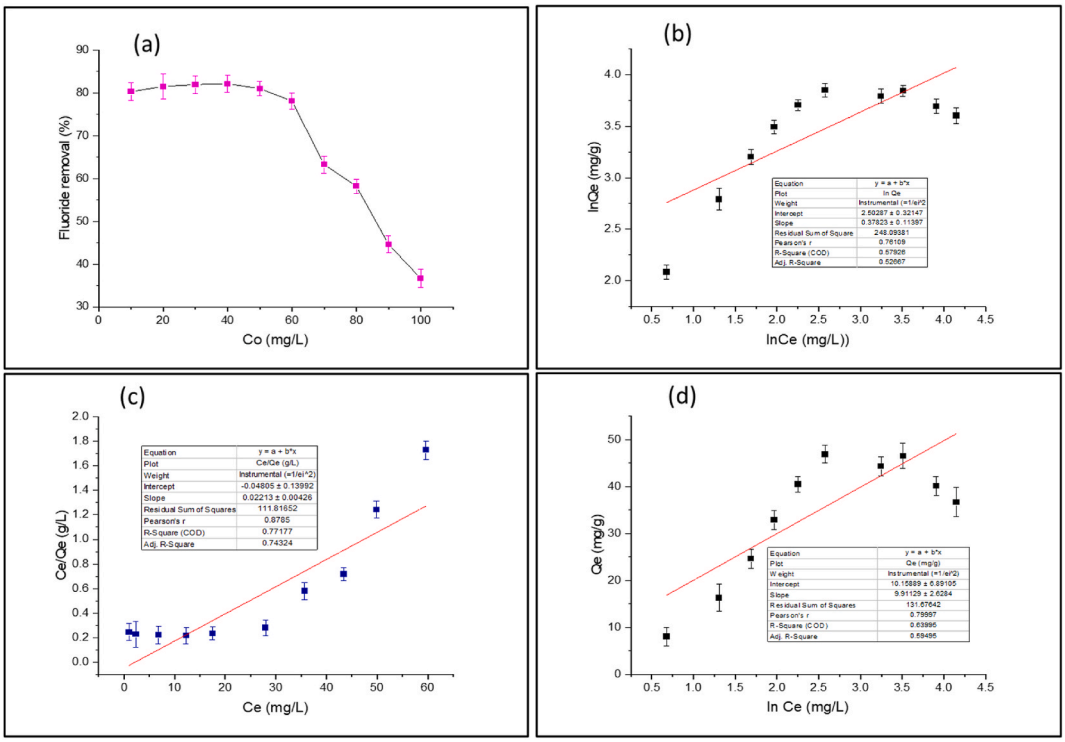

Fig. 8. Equilibrium isotherms for fluoride adsorption onto as synthesized MWCNT-CH (a) plot for the effect of initial fluoride concentration (b) plot of Freundlich isotherm model (c) plot for Langmuir isotherm model and (d) plot of Temkin isotherm model.

Where k_{id} is the rate constant. A plot of Q_t versus $t^{0.5}$ is used to obtain the associated model parameters.

For chemisorption processes involving systems with heterogeneous sorbing surfaces, the Elovich model given by equation (8) best describes adsorption systems, including those with a mild rising tendency [30]

$$Q_t = \frac{1}{\beta}\ln(\alpha.\beta) + \frac{1}{\beta}\ln\,(t) \tag{8}$$

It can be noted that the higher the R^2 values of a kinetic model, the better the experimental data fit into the model. From Table 1, the R^2 values for the pseudo-second-order model for each concentration were higher than the correlation coefficients for the Lagergren Pseudo-first order, Elovich, and Weber Morris kinetic models. Again the calculated adsorption capacities ($Q_{e,cal}$) for the second-order kinetic models were in good agreement with the experimental adsorption capacity ($Q_{e,exp}$) values for the three initial fluoride concentrations.

Hence, pseudo-second-order model well interpreted the data for fluoride adsorption onto the as-synthesized MWCNT-CH composite implying that chemisorption is involved in the rate-limiting step for the adsorption process. The decrease in rate constants with an increase in initial fluoride concentration (Table 1) is attributed to abundant active sites for fluoride adsorption with minimum competition among the few fluoride ions at lower initial concentrations. However, stiff competition ensues between the many fluoride ions for the active sites on the adsorbent at higher initial fluoride concentrations, hence lower adsorption constants [31].

The adsorption mechanism of fluoride onto MWCNT-CH composite was deciphered using FTIR studies before and after adsorption (Fig. 5) and zeta potential measurements (Fig. 6 (b). From Fig. 5, the peak of MWCNT-CH before adsorption at 1684 cm^{-1} and 3200 cm^{-1} was apparent and broad but it almost disappeared after fluoride adsorption, demonstrating that fluoride ions in the solution were exchanged with OH groups on the adsorbent surface. Hence inferring ion exchange mechanism. Again, Fig. 6(b) shows that the zeta potential of the composite decreased with increasing pH value, indicating that the electrical charge at the adsorbent surface depended on the solution pH. Hence, fluoride adsorption was favored by low pH when the adsorbent surface was protonated [32,33]. In this case, electrostatic interaction accounted for mechanism of fluoride adsorption at this pH (3–7) when maximum adsorption of fluoride occurred.

3.5.3. Adsorption equilibrium study for fluoride removal using MWCNT-CH composite

This was studied at initial fluoride concentrations (10–100 mg/L), and the results (Fig. 8 (a) indicated that the fluoride removal efficiency of the MWCNT-CH composite decreased with an increase in initial fluoride concentration. This may be attributed to a deficiency in the availability of active sites on the as-synthesized MWCNT-CH composite at such a higher initial fluoride concentration. Conversely, at lower initial fluoride concentrations (<60 mg/L), the adsorbent adsorption sites were numerous, leading to high fluoride removal efficiency. This finding agrees with results obtained in recent studies [22,34].

The relationship between adsorbent and fluoride ions, as well as the adsorption phenomena, were studied by fitting the equilibrium adsorption data into the Langmuir (1918), Temkin & Pyzhev (1940), and Freundlich (1906) isotherm models as given in equations (8)–(11) respectively. The Langmuir isotherm is given by equation (9) and plot in Fig. 8(c).

$$\frac{1}{Q_e} = \frac{1}{K_L Q_m}\left(\frac{1}{C_e}\right)\frac{1}{Q_m} \tag{9}$$

where: Q_e = sorbed amount of fluoride concentration (mg/g), Q_m = maximum adsorption capacity of the composite for fluoride ions, C_e = equilibrium concentration of aqueous fluoride (mg/L), K_L = measure of the affinity of fluoride ions for the composite.

Again, another critical parameter in the Langmuir isotherm called the separation factor, R_L given by equation (10)

$$R_L = \frac{1}{(1 + K_b C_o)} \tag{10}$$

Generally, a good adsorption process is indicated by $0 < R_L < 1$; linear adsorption is indicated by $R_L = 1$, while $R_L > 1$ and $R_L = 0$ show unfavorable adsorption and irreversible adsorption, respectively [35].

The Temkin isotherm [36] is given by equation (11):

$$Q_e = \frac{RT}{b_T} ln\, K_T + \frac{RT}{b_T} ln\, C_e \tag{11}$$

where: C_e = equilibrium concentration of sorbate, K_T = Temkin isotherm equilibrium binding constant (L/g), R = Universal gas constant (8.314 J/mol/K), T = Temperature at 298 K, b_T = Temkin isotherm constant. A plot of adsorbed fluoride concentration (Q_e) against ln C_e is made (Fig. 8 (d), and the constants are determined from the slope and intercept.

The Freundlich isotherm assumes a varied distribution of adsorption sites on the adsorbent and that the active sites have different affinities for different adsorbates, with each behaving according to the Langmuir isotherm. Freundlich isotherm, therefore, describes multilayer adsorption of fluoride ions over the adsorbent with a heterogeneous surface [37]. A linear form of the Freundlich isotherm is given in equation (12) and plot in Fig. 8(b):

$$Q_e = \ln K_{f+}\frac{1}{n_{ln}} C_e \tag{12}$$

where Q_e = amount of fluoride sorbed per unit weight of the adsorbent (mg/g), C_e = equilibrium concentration of aqueous sorbate (mg/L), K_f = Freundlich constant (L/g) indicative of the relative adsorption capacity of the adsorbent, n = a measure of how an affinity for the sorbate changes with a change in adsorption density.

For a value of n = 1, the Freundlich isotherm becomes a linear isotherm, showing that all the adsorption sites on the adsorbent have equal affinity for the sorbate ions. However, values of n > 1 indicate that affinities of adsorbent for the sorbate ions decrease with increasing adsorption density, while a value of n < 1 means that affinities of adsorbent for the sorbate ions increase with increasing adsorption density [37].

Table 2 summarizes the isotherm fitting results with R^2 values indicating the significance of the model in describing the adsorption phenomena. For this study, the correlation coefficients obtained for Langmuir, Temkin, and Freundlich isotherm models were 0.9991, 0.5792, and 0.5763, respectively. The equilibrium data fitted better in the Langmuir model with an R^2 value of 0.9991, indicating a chemisorption process is involved.

This isotherm assumed that monolayer adsorption on a homogenous surface of the as-synthesized MWCNT-CH composite continues to occur until maximum adsorption capacity reaches saturation with all available adsorption sites occupied by the fluoride ions but without adjacent interactions between sorbed fluoride ions. This study's separation factor, R_L, of 0.043, indicated favorable fluoride adsorption onto the as-synthesized MWCNT-CH composite.

Table 3 presents a comparison of the performance of CNTs and HaP adsorbents in terms of maximum fluoride removal capacity. This comparison reveals that the MWCNT-CH biocomposite is fairly comparable to CNT/HaP composites but is a better adsorbent than hydroxyapatite.

3.5.4. *Fluoride adsorption thermodynamics*

To study the thermodynamics of fluoride adsorption onto MWCNT-CH composite, batch experiments were performed at different temperatures 303, 313, and 323 K using an initial fluoride concentration of 10 mg/L, contact time of 3 h, adsorbent dose of 0.5 g, and pH of 5.25. The thermodynamic parameters were determined using equations 13–15 [22,42].

Equilibrium constant is related to equilibrium concentration by equation 13

$$K = \frac{C_{ad}}{C_e} \tag{13}$$

van't Hoff isotherm is given by equation 14

$$\ln K = -\frac{\Delta H}{R}\left[\frac{1}{T}\right] + \frac{\Delta S}{R} \tag{14}$$

Equation (15) shows the relationship between Gibbs free energy change and the equilibrium constant for fluoride adsorption onto the MWCNT-CH composite.

$$\Delta G = -RTlnK \tag{15}$$

where K, Δ H (J/mol), R (8.314 J/mol K), T(K), Δ S (J/mol/K), Δ G (J/mol), C_e (mg/L), and C_{ad} (mg/L) are the equilibrium constant, enthalpy change, molar gas constant, absolute temperature, entropy change, Gibbs free energy change, the concentration of fluoride ions in solution at equilibrium and amount of fluoride sorbed at equilibrium, respectively. A plot of the van't Hoff isotherm (eqn. (14)) is given in Fig. S3 (supporting information).

For this study, the values of Δ G decreased with an increase in temperature (Table 4) for all the initial fluoride concentrations.

Table 2
Adsorption isotherm parameters of fluoride using MWCNT − CH composite (N = 3, Relative standard deviation, RSD <5%).

Isotherm	Parameter	Value
	Q_m (mg/g)	41.37
	K_L (L/mg)	2.24
Langmuir	R_L	0.043
	R^2	0.9991
Temkin	R^2	0.57924
	$K_{T(}$L/g)	3.22
	B	9.10781
	b_T	272
Freundlich	K_f (mg/g) $(L/mg)^{1/n}$	11.26
	N	2.57
	R^2	0.57631
	1/n	0.38889

Definition of equation terms: Q_e = concentration of fluoride ions sorbed at equilibrium, C_e = equilibrium concentration of fluoride ions, R_L = separation factor, Q_m = maximum adsorption capacity corresponding to monolayer coverage on the surface of the adsorbent, K_L = Langmuir constant, which is related energy of adsorption, K_F and 1/n are Freundlich constants while K_T and B are Temkin constants.

Table 3
Comaprison of MWCNT-CH with other CNT/HaP adsorbents.

Adsorbent	Adsorption Capacity (mg/g)	pH	Reference
Bare Hydroxyapatite (HaP)	2.63	4–11	[38]
HaP modified with Cationic Surfactants	9.37	4–11	[39]
HaP modified with H_3PO_4	4.52	7.5	[33]
Aligned CNTs	4.5	7	[32]
SWCNT	58.92	6	[40]
MWCNT/HAp	39.22	–	[41]
CNT/HaP	11.05	3–6	[9]
MWCNT-CH biocomposite	41.70	7	This study

Table 4
Thermodynamic Parameters for Adsorption of Fluoride onto as-synthesized MWCNT-CH Biocomposite.

Initial fluoride concentration (mg/L)	Δ H (J/mol)	Δ S (J/mol/K)	Δ G (J/mol)		
			303 K	313K	323K
10	13.950	65.760	−6449	−6661.84	−6874.68
50	11.905	42.74	−1060.56	−1095.56	−1130.56
100	21.493	63.75	−486.19	−502.24	−518.29

The negative Δ G values for all the temperatures and initial fluoride concentrations mean that fluoride adsorption onto the as-synthesized MWCNT-CH composite was feasible and imprudent. This means that at high temperatures, the value of ΔG decreased with consequent improvement in fluoride adsorption. This phenomenon is because higher temperature lowers the solution's volume expansion and viscosity, which increases the magnitude of mass transfer from the liquid phase to the solid interface [22,34]. Generally, values of $0 \leq \Delta G \leq -20,000$ J/mol indicate physiadsorption process whereas $-80{,}000 \leq \Delta G \leq -400{,}000$ J/mol show chemiadsorption. In the present study, the values of ΔG were in the range of 0 J/mol to $-20,000$ J/mol, indicating that the fluoride removal process by the as-synthesized MWCNT-CH composite involved physisorption.

At the same time, the positive values of ΔH obtained in this study were below 40 kJ/mol, signaling that the adsorption process is physisorption and endothermic [34]. The value ΔS decreased with an increase in initial fluoride concentration. The positive value of ΔS warranted the randomness increase at the solid-liquid interface. The increase in randomness is due to the displacement of sorbed water molecules by the fluoride ions to attain more translational entropy than is lost by the fluoride ions, thereby allowing for a high degree of randomness in the system [43].

3.5.5. *Effect of Co-existing anions*

Common anions that occur in groundwater and could affect fluoride removal from water due to the investigated competitive

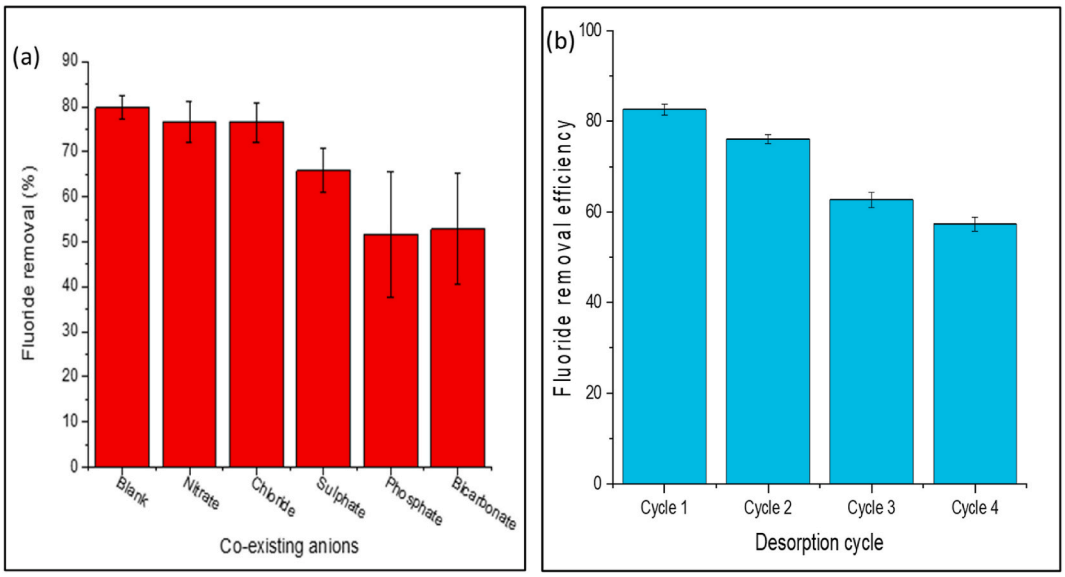

Fig. 9. (a) Effect of co-existing anions on fluoride removal using MWCNT-CH composite (b) Desorption efficiency of the as-synthesized MWCNT-CH composite.

inhibition are SO_4^{2-}, NO_3^-, Cl^-, PO_4^{3-}, and HCO_3^- on fluoride removal using the as-synthesized MWCNT-CH composite (Fig. 9 (a). It was observed that $PO_4^{3-}$and HCO_3^- had severe adverse effects on fluoride removal efficiency of the as-synthesized MWCNT-CH composite while the SO_4^{2-}, NO_3^-, and Cl^- had a slight effect on fluoride adsorption. The adverse effects of the HCO_3^- could be due to similarity in size and charge while that of PO_4^{3-} could be due to anion hydrolysis leading to the release of hydroxide ions, which raises the pH of the solution (eqn. (16)–(18)).

$$PO_4^{3-}(aq) + H_2O\ (l) \rightleftharpoons HPO_4^{2-}(aq) + OH^-(aq)\ \ K_b = 1.0 \times 10^{-2} \quad (16)$$

$$HPO_4^{2-}(aq) + H_2O\ (l) \rightleftharpoons H_2PO_4^-(aq) + OH^-(aq)\ \ K_b = 1.6 \times 10^{-7} \quad (17)$$

$$H_2PO_4^{2-}(aq) + H_2O\ (l) \rightleftharpoons H_3PO_4\ (aq) + OH^-(aq)\ \ K_b = 1.3 \times 10^{-12} \quad (18)$$

The increased pH creates negative charges on the adsorbent, causing electrostatic repulsion of incoming fluoride ions, reducing fluoride adsorption efficiency [9,44].

3.5.6. Desorption and reusability study

In this study, spent adsorbent was regenerated in four cycles by desorption using a 0.1 M sodium hydroxide solution to assess its sustainability in fluoride removal from water.

Unfortunately, the adsorption efficiency in each cycle decreased, as shown in Fig. 9 (b) ($p < 0.05$). However, the composite still had 57.3% effectiveness for fluoride removal in the fourth cycle. Consequently, the as-synthesized MWCNT-CH composite can be a reusable adsorbent for the remediation of fluoride-ladened water.

3.5.7. RSM study of fluoride adsorption onto as -synthesized MWCNT-CH composite

Fig. 10 shows the 3D surface plots and graphical representations of the effect of two independent process variables on fluoride adsorption when all the other process variables were kept constant. The incline of the 3D surface plots indicates the strength of the interaction of the two independent variables under consideration [45]. The interactive effect of adsorbent dose and initial fluoride concentration (Fig. 10 (a) shows an inclined curve indicating a significant interplay between the two factors. An increase in adsorbent dose resulted in a corresponding increase in fluoride removal efficiency due to an increased number of active sites for fluoride adsorption. On the other hand, an increase in initial fluoride concentration had a negative effect. In fact, with a high initial fluoride

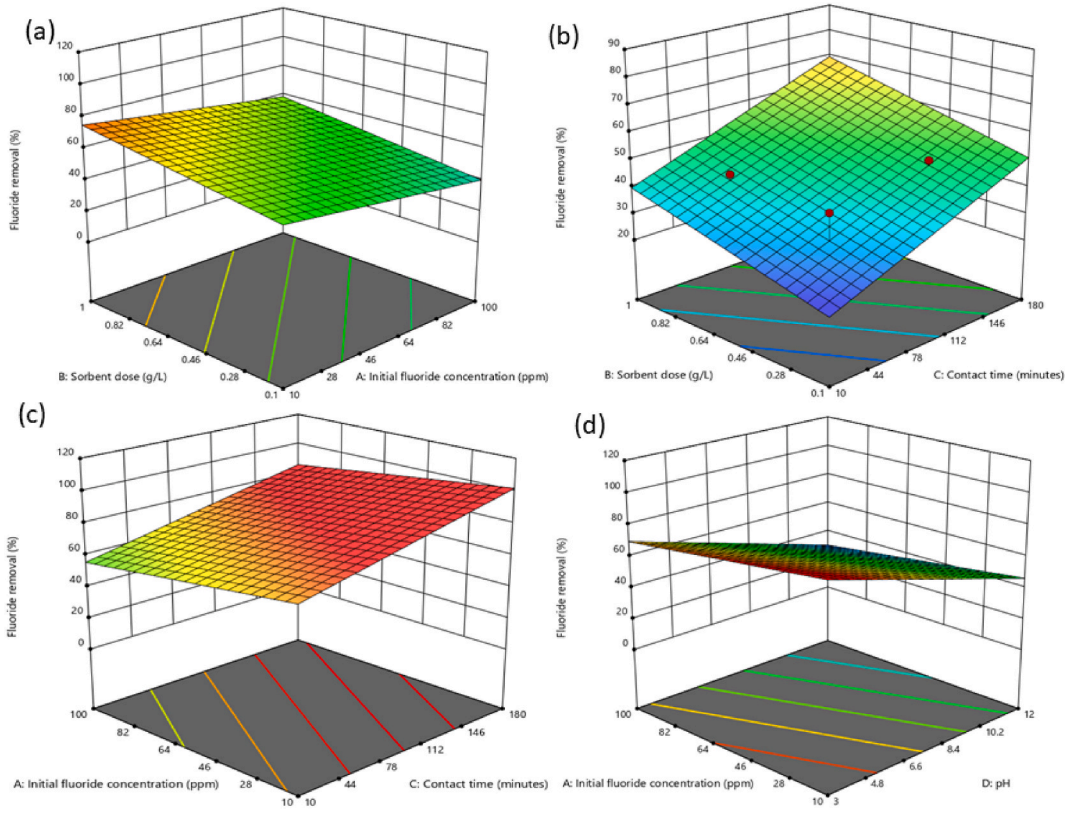

Fig. 10. 3D surface plot showing the effect of (a) adsorbent dose and initial fluoride concentration (b) Adsorbent dose and contact time (c) initial fluoride concentration and contact time (d) initial fluoride concentration and pH.

concentration, fluoride adsorption capacity reduces due to the saturation of the active sites with fluoride ions on the adsorbent surface, and no further adsorption takes place [45]. Therefore, an increased adsorbent dose from 0.1 g to 1.0 g and a low initial fluoride concentration (10 mg/L) resulted in a sustained fluoride removal percentage of up to 75%.

Similarly, an interactive plot for adsorbent dose and contact time displayed in Fig. 10 (b) is very much inclined, showing that the interplay between the factors is significant. According to Fig. 10 (b), both adsorbent dose and contact time had significant effects on fluoride removal, with both factors increasing fluoride adsorption efficiency.

Fig. 10 (c) displays a significant interaction between initial fluoride concentration and contact time, with an increase in contact time having the most significant effect on fluoride removal efficiency. Their combined effect resulted in the highest fluoride removal efficiency of approximately 80.2% at an initial fluoride concentration of 10 mg/L and contact time of 78 min.

A low pH (4.8) favored fluoride adsorption, but cooperatively, an adsorption efficiency of 39% was attained at an initial fluoride concentration of 10 mg/L. In addition, the adsorbent surface was protonated at low pH, thereby electrostatically attracting fluoride ions (Fig. 10 (d).

The most excellent cooperative effect was exhibited in the interactive plot for the as-synthesized MWCNT-CH dose and contact time (Fig. 10 (c), with an increase in both factors improving fluoride removal tremendously. An increase in MWCNT-CH dose from 0.1 to 0.46 g and contact time from 10 to 78 min resulted in a fluoride removal efficiency of 69%. Comparable results were revealed by Ref. [44]. From the optimization study, maximum fluoride removal can be achieved with an initial fluoride concentration of 10 mg/L, contact time of 78 min, pH of 5, and adsorbent dose of 0.46 g/L. The results discussed here indicate that each of the four factors affects fluoride removal efficiency differently.

3.5.8. Model development for adsorption of fluoride onto the as-synthesized MWCNT-CH composite

Fluoride adsorption onto the as-synthesized MWCNT-CH was optimized using the central composite design (CCD) approach. An experimental design matrix composed of thirty experiments was developed using the CCD method. In addition, a multivariable data-driven model was developed to predict fluoride removal efficiency for different amounts of the process variables. The linear model in equation (19) shows the numerical relationships between independent variables and percentage fluoride removal

$$Fluoride\ removal\ (\%) = +73.86225 - 0.178259\,A + 20.66667B + 0.175412C - 4.37926D \quad (19)$$

The independent process variables *A, B, C,* and *D* are initial fluoride concentration, contact time, pH, and amount of the as-synthesized MWCNT-CH composite. Positive signs of the coefficients in the model show synergistic effects, while the negative sign of coefficients denotes opposing or antagonizing effects.

Analysis of variance (ANOVA) for the fluoride removal efficiency by the as-synthesized MWCNT-CH composite (Table 5) suggests that initial fluoride concentration, contact time, pH, and adsorbent dose were all significant model terms. These terms were checked with p-values and F-values. Therefore, A, B, C, and D are significant model terms. It can be seen from Table 5 that the variables with the largest effect ($p < 0.05$) on fluoride removal by the composite were the linear terms in order of pH > contact time > adsorbent dose > initial fluoride concentration.

Furthermore, the predicted coefficient of determination R^2 of 0.50 is in reasonable agreement with adjusted R^2 of 0.62, with a difference <0.2 and p-value (<0.05) and F-value of 12.71, indicating that the model terms are significant. The adequacy of precision measures signal-to-noise ratio with a value greater than four being desirable. Therefore, the adequacy of 13.40 obtained in this study shows that the developed model can navigate the design space since there is a sufficient signal in the model with negligible noise (errors). A plot of predicted values Vs. actual values (Fig. 11) also signify that the developed model is an earnest predictor of fluoride adsorption onto the as-synthesized MWCNT-CH composite. As seen in Fig. 11, most predicted values were near the experimental data.

Hence, the model (Eqn. (19)) could be practically and reliably applied for predicting fluoride removal percentage using the as-synthesized MWCNT-CH biocomposite at the stated independent variable levels [46].

3.5.9. Validation of the model for fluoride adsorption process onto as-synthesized MWCNT-CH composite

Three fluoride adsorption experiments were conducted at the optimized values of the process variables for maximum fluoride removal of 80.21% by the as-synthesized MWCNT-CH composite of initial fluoride concentration = 10 mg/L, pH = 5.25, and adsorbent dose = 0.5 g at a contact time of 78 min.

The experiments were repeated three times to verify the prediction, and the results are given in Table 6. The experimental values for fluoride removal using MWCNT-CH composite are in good agreement with the model-predicted values with a standard deviation (S.D) ≤ 0.05.

4. Conclusion

The synthesis of a multi-walled carbon nanotube decorated with hydroxyapatite from cattle horns by the facile chemical method was achieved for the adsorption of fluoride ions from water. This method is environmentally sound as it uses low temperature, ordinary pressure, and an inexpensive source of hydroxyapatite. The kinetic experiment showed that fluoride adsorption onto MWCNT-CH was majorly governed by chemisorption while the equilibrium isotherm was welled modeled by the Langmuir equation, indicating monolayer adsorption with a maximum adsorption capacity of 41.7 mg/g^{-1}. Thermodynamic data showed that the adsorption process is spontaneous and endothermic, with increased randomness at the solid-liquid interface. RSM study showed that the optimum values for maximum fluoride removal by the as-synthesized MWCNT-CH were initial fluoride concentration = 10 mg/L, pH = 5.25, sorbent

Table 5
Analysis of variance for the quadratic model for fluoride adsorption using MWCNT-CH composite.

Source	Sum of Squares	df	Mean Square	F-value	p-value	
Model	4568.99	4	1142.25	12.71	<0.0001	significant
A-Initial fluoride concentration	386.08	1	386.08	4.30	0.0487	
B-Adsorbent dose	518.94	1	518.94	5.77	0.0240	
C-Contact time	1333.85	1	1333.85	14.84	0.0007	
D-pH	2330.12	1	2330.12	25.93	<0.0001	
Residual	2246.83	25	89.87			
Lack of Fit	2027.42	20	101.37	2.31	0.1797	not significant
Pure Error	219.40	5	43.88			
Cor Total	6815.81	29				

According to the F-value, the degree of influence of the variables was in the order of pH > contact time > adsorbent dose > initial fluoride concentration.

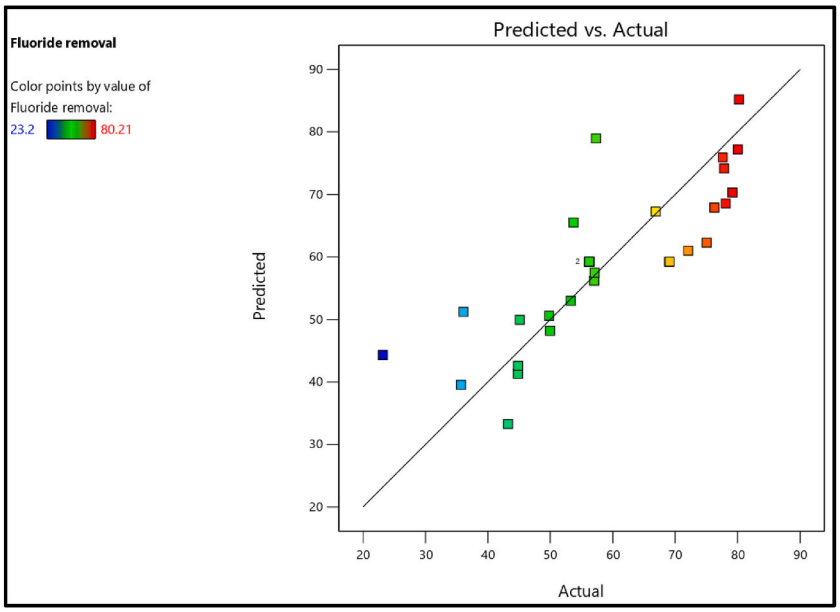

Fig. 11. Comparison of the Actual response Vs Predicted fluoride adsorption response.

Table 6
Model validation at optimum conditions.

Experiment	Optimum parameters				Fluoride removal %		
	Initial F^-conc. (mg/L)	pH	dose:(g)	Contact time (min.)	Experimental	Predicted	SD
1	10.00	5.25	0.50	78.5	79.68	79.70	0.02
2	10.02	5.50	0.52	80.0	79.61	79.63	0.02
3	10.01	5.30	0.51	78.4	79.03	79.07	0.04

dose = 0.5 g, and contact time of 78 min. Adsorption mechanism involved ion exchange where F- ions replaced some of the OH^- ions on the composite and $\pi-$ electrostatic interaction and hydrogen bonding. The presence of $PO_4^{3-}$and HCO_3^- had severe adverse effects on fluoride removal efficiency, while SO_4^{2-}, NO_3^-, and Cl^- in the water had little effect on fluoride adsorption efficiency. Furthermore, the MWCNT-CH composite showed good desorption properties and reusability. Hence, the as-synthesized MWCNT-CH composite could be a useful fluoride adsorbent for the remediation of fluoride-contaminated water.

Author contribution statement

Walter Ojok: Conceived and designed the experiments; Performed the experiments; Analyzed and interpreted the data; Wrote the paper.

James Bolender, William Wanasolo, Brenda Moodley: Conceived and designed the experiments; Contributed reagents, materials,

analysis tools or data.

John Wasswa, Emmanuel Ntambi: Conceived and designed the experiments.

Funding statement

This work was supported by a Ph.D. Scholarship by the German Academic Exchange Service (DAAD) (Grant No. 91672385), Muni University, and the African-German Network of Excellence in Science.

Data availability statement

Data will be made available on request.

Declaration of interest's statement

The authors declare no conflict of interest.

Acknowledgments

The authors would like to acknowledge the technical support by the School of Chemistry and Physics, University of KwaZulu-Natal, Westville Campus, and Department of Chemistry, Mbarara University of Science and Technology as well as Muni University Management for permitting the principal author (W.O) to travel for fellowship. Finally, W.O is grateful to all members of the Analytical/Physical Chemistry Research Groups for their enormous help in accessing the various laboratories and with instrumentation. W.O is a Ph.D. student at the Department of Chemistry, Mbarara University of Science and Technology, Mbarara (Uganda), and was an AGNES research fellow at the School of Chemistry and Physics, University of KwaZulu-Natal, Westville Campus.

Appendix A. Supplementary data

Supplementary data to this article can be found online at https://doi.org/10.1016/j.heliyon.2023.e14341.

References

[1] R. Araga, C.S. Sharma, One step direct synthesis of multiwalled carbon nanotubes from coconut shell derived charcoal, Mater. Lett. 188 (2017) 205–207.
[2] A.I. Osman, C. Farrell, H. Ala'a, J. Harrison, D.W. Rooney, The production and application of carbon nanomaterials from high alkali silicate herbaceous biomass, Sci. Rep. 10 (2020) 1–13.
[3] Y. Wang, C. Teng, T. Hu, Wang, J. Total conversion from graphite to few-layer graphene nanocomposite, Carbon Trends 2 (2021), 100017.
[4] T.W. Ebbesen, Carbon Nanotubes: Preparation and Properties, CRC press, 1996.
[5] M.E. David, et al., Synthesis and characterization of multi-walled carbon nanotubes decorated with hydroxyapatite, Fullerenes, Nanotub. Carbon Nanostruct. 29 (2021) 423–430.
[6] W. Ojok, W. Wanasolo, J. Wasswa, J. Bolender, E. Ntambi, Hydrochemistry and fluoride contamination in Ndali-Kasenda crater lakes, Albertine Graben: assessment based on multivariate statistical approach and human health risk, Groundw. Sustain. Dev. 100650 (2021).
[7] S. Ali, S.K. Thakur, A. Sarkar, S. Shekhar, Worldwide contamination of water by fluoride, Environ. Chem. Lett. 14 (2016) 291–315.
[8] P. Mondal, M.K. Purkait, Preparation and characterization of novel green synthesized iron–aluminum nanocomposite and studying its efficiency in fluoride removal, Chemosphere 235 (2019) 391–402.
[9] Q. Tang, T. Duan, P. Li, P. Zhang, D. Wu, Enhanced defluoridation capacity from aqueous media via hydroxyapatite decorated with carbon nanotube, Front. Chem. 6 (2018) 104.
[10] J. Liang, et al., Facile synthesis of alumina-decorated multi-walled carbon nanotubes for simultaneous adsorption of cadmium ion and trichloroethylene, Chem. Eng. J. 273 (2015) 101–110.
[11] T.-Y. Sun, Y. Hao, C.-T. Lin, L. Wang, L.-F. Huang, Unraveling the strong coupling between graphene/nickel interface and atmospheric adsorbates for versatile realistic applications, Carbon Trends 2 (2021), 100013.
[12] M. Chen, et al., Fabrication of multiwalled carbon nanotubes/carrageenan-chitosan@ Ce and Sr substituted hydroxyapatite biocomposite coating on titanium: in vivo bone formation evaluations, J. King Saud Univ. 32 (2020) 1175–1181.
[13] M. Matandabuzo, P.A. Ajibade, Synthesis and surface functionalization of multi-walled carbon nanotubes with imidazolium and pyridinium-based ionic liquids: thermal stability, dispersibility and hydrophobicity characteristics, J. Mol. Liq. 268 (2018) 284–293.
[14] F.S.A. Khan, et al., Functionalized multi-walled carbon nanotubes and hydroxyapatite nanorods reinforced with polypropylene for biomedical application, Sci. Rep. 11 (2021) 1–10.
[15] C. Zhang, S. Wang, Z. Zhan, A.M. Amin, B. Tan, Synthesis of MWCNT-based hyper-cross-linked polymers with thickness-tunable organic porous layers, ACS Macro Lett. 8 (2019) 403–408.
[16] R. Barabás, et al., Graphene oxides/carbon nanotubes–hydroxyapatite nanocomposites for biomedical applications, Arabian J. Sci. Eng. 45 (2020) 219–227.
[17] Y. Wang, et al., Analysis and identification of different animal horns by a three-stage infrared spectroscopy, Spectrochim. Acta Part A Mol. Biomol. Spectrosc. 83 (2011) 265–270.
[18] I.I. Ahmed, A.A. Buhari, S. Abdulkareem, T. Yahaya, J.A. Adebisi, Thermochemical characterization of horns and hooves for carbonitriding treatment, Mater. Perform. Charact. 9 (2020) 605–613.
[19] N.A.M. Barakat, M.S. Khil, A.M. Omran, F.A. Sheikh, H.Y. Kim, Extraction of pure natural hydroxyapatite from the bovine bones bio waste by three different methods, J. Mater. Process. Technol. 209 (2009) 3408–3415.
[20] P. Nelson, Index to EPA Test Methods, United States Environmental Protection Agency, Region I, 2003.
[21] D. Dayananda, V.R. Sarva, S.V. Prasad, J. Arunachalam, N.N. Ghosh, Preparation of CaO loaded mesoporous Al 2 O 3 : efficient adsorbent for fluoride removal from water national centre for compositional characterization of materials (CCCM), bhabha atomic, Chem. Eng. J. 248 (2014) 430–439.

[22] W. Ojok, et al., Synthesis and characterization of hematite biocomposite using cassava starch template for aqueous phase removal of fluoride, Carbohydr. Polym. Technol. Appl. 4 (2022), 100241.
[23] N.A. Medellin-Castillo, et al., Removal of fluoride from aqueous solution using acid and thermally treated bone char, Adsorption 22 (2016) 951–961.
[24] J. Lin, Y. Wu, A. Khayambashi, X. Wang, Y. Wei, Preparation of a novel CeO 2/SiO 2 adsorbent and its adsorption behavior for fluoride ion, Adsorpt. Sci. Technol. 36 (2018) 743–761.
[25] S. Lagergren, S. Lagergren, S.Y. Lagergren, K. Sven, Zurtheorie der sogenannten adsorption gelösterstoffe, 1898.
[26] Y.-S. Ho, G. McKay, Pseudo-second order model for sorption processes, Process Biochem. 34 (1999) 451–465.
[27] B. Likozar, D. Senica, A. Pavko, Comparison of adsorption equilibrium and kinetic models for a case study of pharmaceutical active ingredient adsorption from fermentation broths: parameter determination, simulation, sensitivity analysis and optimization, Braz. J. Chem. Eng. 29 (2012) 635–652.
[28] P. Atkins, J. De Paula, Keeler, J. *Atkins' Physical Chemistry*, Oxford university press, 2018.
[29] W.J. Weber, J.C. Morris, Kinetics of adsorption on carbon from solution, J. Sanit. Eng. Div. 89 (1963) 31–60.
[30] S. Roginsky, Y.B. Zeldovich, The catalytic oxidation of carbon monoxide on manganese dioxide, Acta Phys. Chem. USSR 1 (1934) 2019.
[31] S.I. Alhassan, et al., Fluoride removal from water using alumina and aluminum-based composites: a comprehensive review of progress, Crit. Rev. Environ. Sci. Technol. 1 (2020) 35.
[32] Y.-H. Li, et al., Adsorption of fluoride from water by aligned carbon nanotubes, Mater. Res. Bull. 38 (2003) 469–476.
[33] N.S. Yapo, et al., Removal of fluoride in groundwater by adsorption using hydroxyapatite modified Corbula trigona shell powder, Chem. Eng. J. Adv. 12 (2022), 100386.
[34] Y. Yang, et al., Adsorption property of fluoride in water by metal organic framework: optimization of the process by response surface methodology technique, Surface. Interfac. 28 (2022), 101649.
[35] I. Langmuir, The adsorption of gases on plane surfaces of glass, mica and platinum, J. Am. Chem. Soc. 40 (1918) 1361–1403.
[36] M.J. Temkin, V. Pyzhev, Recent Modifications to Langmuir Isotherms, 1940.
[37] H.M.F. Freundlich, Over the adsorption in solution, J. Phys. Chem. 57 (1906) 1100–1107.
[38] M. Mourabet, et al., Removal of fluoride from aqueous solution by adsorption on hydroxyapatite (HAp) using response surface methodology, J. Saudi Chem. Soc. 19 (2015) 603–615.
[39] M. Jiménez-Reyes, M. Solache-Ríos, Sorption behavior of fluoride ions from aqueous solutions by hydroxyapatite, J. Hazard Mater. 180 (2010) 297–302.
[40] M.H. Dehghani, et al., Adsorptive removal of fluoride from aqueous solution using single-and multi-walled carbon nanotubes, J. Mol. Liq. 216 (2016) 401–410.
[41] Z. Ruan, et al., Synthesis of hydroxyapatite/multi-walled carbon nanotubes for the removal of fluoride ions from solution, Appl. Surf. Sci. 412 (2017) 578–590.
[42] S. Raghav, D. Kumar, Comparative kinetics and thermodynamic studies of fluoride adsorption by two novel synthesized biopolymer composites, Carbohydr. Polym. 203 (2019) 430–440.
[43] S. Raghav, S. Nehra, D. Kumar, Biopolymer scaffold of pectin and alginate for the application of health hazardous fluoride removal studies by equilibrium adsorption, kinetics and thermodynamics, J. Mol. Liq. 284 (2019) 203–214.
[44] P. Pillai, S. Dharaskar, M. Khalid, Optimization of fluoride removal by Al doped ZnO nanoparticles using response surface methodology from groundwater, Chemosphere 284 (2021), 131317.
[45] M.-J. Kim, S.-H. Hong, J.-I. Lee, C.-G. Lee, S.-J. Park, Removal of fluoride from water using thermally treated dolomite and optimization of experimental conditions using response surface methodology, Desalination Water Treat. 155 (2019) 311–320.
[46] R.T. Iwar, K. Ogedengbe, B.O. Ugwudike, Groundwater fluoride removal by novel activated carbon/aluminium oxide composite derived from raffia palm shells: optimization of batch operations and field-scale point of use system evaluation, Results Eng. 14 (2022), 100407.